A Repeater-Based Dynamic Wireless Power Transfer System With Controllable Detuning Rate for a Constant Output Profile

Wenjing Xiong, *Member, IEEE*, Jiawei Tan, Zixi Liu, *Member, IEEE*, Qi Zhu, Yao Sun, *Member, IEEE*, Mei Su, *Member, IEEE*, and Bo Long

***Abstract*—The dynamic wireless power transfer (DWPT) system is an ideal solution for electric vehicles as it can maintain the power supply and reduce the battery volume. However, its adoption in electric vehicle charging has been limited due to the high installation costs, low charging efficiency, and significant power fluctuations. To address these issues, a repeater-based DWPT system with a controllable detuning rate method is proposed to achieve constant output power during movement. The switch-controlled capacitor is introduced in the repeater coil to adjust its detuning rate dynamically. Based on the relationship between the output power and the mutual inductances among the active, repeater, and receiver coils, the detuning rate is controlled to reduce power fluctuations. Moreover, increasing the detuning rate under no-load conditions reduces the losses in the repeater coil. A down-sized experimental prototype of the proposed DWPT system was built, and the experimental results show that it can maintain output power with fluctuations of less than 4.8% and an efficiency of approximately 85% throughout the dynamic process. Furthermore, constant power output is maintained even when the mutual inductance between the repeater coil and the active coil varies by up to 25%.**

***Index Terms*—Constant power output, controllable detuning rate, dynamic wireless power transfer (DWPT) system, switch-controlled capacitor.**

I. Introduction

WIRELESS power transfer is an emerging technology that has rapidly developed with the advancement of power electronics technology. Compared to the wired power transfer, it offers advantages such as greater convenience, higher security, and lower maintenance costs [1], [2], [3]. Depending on whether the receiver coil moves, the wireless power transfer system can be classified into the static wireless power transfer (SWPT) system and the dynamic wireless power transfer (DWPT) system. SWPT has been widely applied in various fields, such as electric vehicles [4], mobile electronic devices [5], drones [6], and implantable medical devices [7]. However, the need for high-capacity batteries and long charging times presents challenges for the widespread adoption of SWPT in the field of electric vehicles [8], [9], [10].

The DWPT system has become a research hotspot in the field of wireless charging due to its high safety, ability to save charging time and space, and its potential for charging during vehicle operation, offering broad application prospects. During the operation of an electric vehicle, the active coil beneath the road provides real-time electrical energy to the receiver coil [8], [9]. If there is a lateral or longitudinal deviation between the receiver coil and the active coil, the coupling coefficient between the coils will change, leading to variations in the system's output power and affecting the overall system's efficiency. Therefore, effective measures must be taken to ensure the system outputs constant power during the vehicle's movement [10]. Based on the current development status of the DWPT systems, their widespread adoption faces several challenges: 1) high system installation costs; 2) low system output efficiency; 3) large output power fluctuations; 4) low tolerance for changes in mutual inductance and load [11], [12].

To accommodate the aforementioned issues, extensive research has been conducted on various aspects, including coil structure, control methods, and topology design. The multicoils, such as the rectangular-solenoidal pad (RSP) coil, solenoid and a planar square coil with a third coil (SPS-TC) coil, and orthogonal magnetic structure receiving coil (OMSRC) coil proposed in [13], [14], [15], improve the system's tolerance to misalignment by increasing the coupling area through the magnetic field superposition. However, these designs not only increase the copper losses in the coils, thereby reducing the overall system's efficiency but also raise the installation costs. In [16], the charging region of the receiver coil is detected by monitoring the input current of the inverter and load, which in turn controls the activation and deactivation of the coupled and

Received 28 August 2024; revised 29 November 2024 and 20 January 2025; accepted 17 February 2025. Date of publication 21 February 2025; date of current version 14 April 2025. This work was supported in part by the National Natural Science Foundation of China under Grant 52377202 and Grant 62192754 and in part by the Hunan Provincial Natural Science Foundation of China under Grant 2023JJ30689 and Grant 2024JJ1011. Recommended for publication by Associate Editor A. Safaee. *(Corresponding author: Zixi Liu.)*

Wenjing Xiong, Jiawei Tan, Yao Sun, and Mei Su are with the School of Automation, Central South University, Changsha 410083, China, and also with the Hunan Provincial Key Laboratory of Power Electronics Equipment and Grid, Central South University, Changsha 410083, China (e-mail: xiongwj@csu.edu.cn; tanjiawei990328@csu.edu.cn; yaosun@csu.edu.cn; sumeicsu@csu.edu.cn).

Zixi Liu, Qi Zhu, and Bo Long are with the Beijing Xiaomi Mobile Software Company Ltd., Beijing 100085, China (e-mail: liuzixi1@xiaomi.com; zhuqi3@xiaomi.com; longbo@xiaomi.com).

Color versions of one or more figures in this article are available at https://doi.org/10.1109/TPEL.2025.3544309.

Digital Object Identifier 10.1109/TPEL.2025.3544309

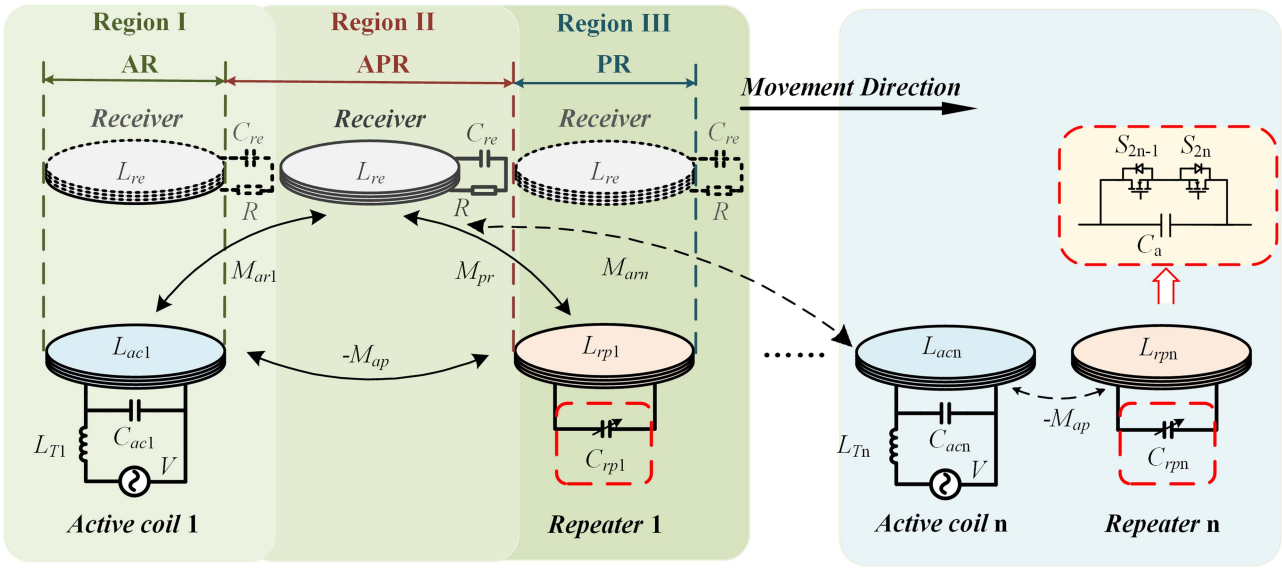

Fig. 1. Overall structure of the proposed system.

uncoupled coils. In [17], the autotuning control is employed to adjust the current in both the coupled and uncoupled coils. In [18], the switches are used to alternate between SS and LCL resonant networks, enabling the system to exhibit varying output characteristics under different coupling coefficients. Although these three control methods improve the system's efficiency, the output power fluctuates significantly as the receiver coil moves. A three-resonator WPT system has been proposed to reduce installation costs, but the improvement in coupling tolerance remains limited [19]. The concept of the detuning rate was introduced to allow the overall system to operate in a detuned state, significantly reducing the no-load losses of the repeater coil and thereby improving the system's efficiency and misalignment tolerance. However, the system's reliance on high-precision parameters presents challenges for broader adoption [20].

This article proposes a DWPT system based on a repeater coil with a controllable detuning rate to address the aforementioned issues. The main innovations of the proposed system are summarized as follows.

1) A wide-range constant power output is achieved by replacing the resonant capacitor in the repeater coil with a switch-controlled capacitor (SCC) to adjust the detuning rate of the system. Consequently, a new control variable is available.
2) Based on the external characteristics of the SCC and the definition of the detuning rate, the system model is simplified. A method for characterizing the system's output characteristics based on the detuning rate is proposed.
3) A control method based on the system model is proposed, enabling a constant power output during dynamic mutual inductance variations. This method achieves a constant output profile by solely detuning the repeater coils and optimizes the system's efficiency.

The rest of this article is organized as follows. Section II presents the system model of the proposed DWPT. In Section III, the detuning rate is defined, and the control strategy for adjusting the detuning rate is analyzed. In Section IV, an experimental prototype is built to verify the feasibility of the proposed DWPT system. Finally, Section V concludes this article.

II. System Structure and Modeling

A. Overall Structure of the Repeater-Based DWPT System

The overall structure of the repeater-based dynamic wireless power transfer system is shown in Fig. 1. The proposed system adopts an alternating arrangement of the active coil units and the repeater coil units. Each active coil unit consists of an ac power supply V, an active coil L_{aci}, a resonant inductor L_{Ti}, and a resonant capacitor C_{aci} (where $i = 1, 2, 3, \ldots, n$). Each repeater coil unit consists of a repeater coil L_{rpi} and a SCC C_{rpi} containing two switches S_{2i-1} and S_{2i}. The receiver coil circuit consists of a receiver coil L_{re}, a resonant capacitor C_{re}, and a load R.

Additionally, M_{arn} is the mutual inductance between the active coil n and the receiver coil, M_{ap} is the mutual inductance between the repeater coil and the active coil, and M_{pr} is the mutual inductance between the receiver coil and the repeater coil. Due to the direction of the magnetic flux received by the receiver coil being opposite to that through the repeater coil, a minus sign precedes M_{ap}. The active coil transmits power directly or via the repeater coil to the receiver coil. The repeater coil transfers the power from the active coil to the receiver coil through mutual inductance M_{pr}. The receiver coil receives power from both the active coil and the repeater coil, delivering it to the load through a resonant network.

The dynamic process of the system can be divided into three distinct charging modes based on the position of the receiver coil, as shown in Fig. 1. When the receiver coil is in Region I, Region II, or Region III, the system operates in the active-receiver (AR), active-repeater-receiver (APR), and repeater-receiver (PR) charging modes, respectively. In the AR

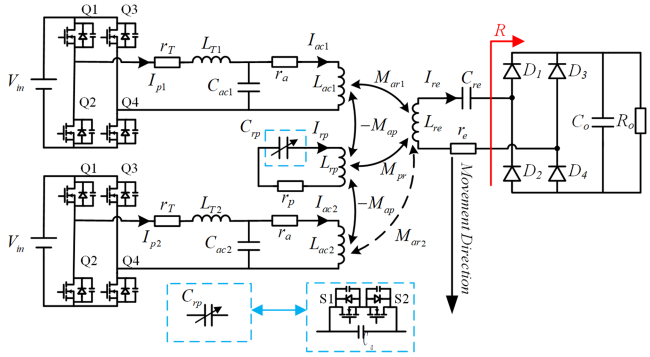

Fig. 2. Equivalent circuit unit of the proposed DWPT system.

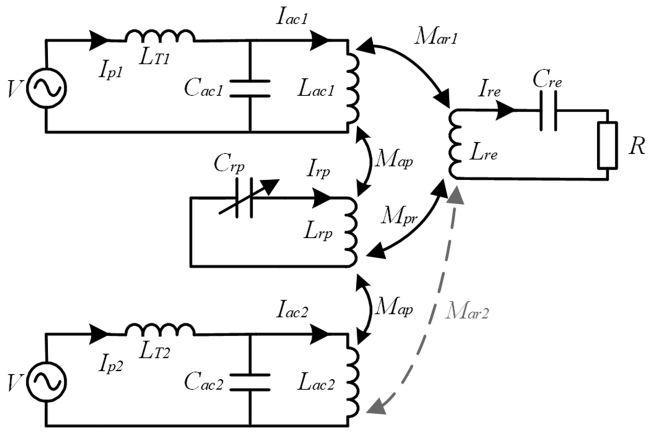

Fig. 3. Equivalent circuit of the DWPT system in PR mode.

mode, power is supplied solely by the active coil unit. In the APR mode, both the active coil unit and the repeater coil unit provide power. In the PR mode, power is supplied exclusively by the repeater coil unit.

During operation, the charging mode follows the sequence AR-APR-PR-APR-AR. Additionally, the closer the receiver coil is to the repeater coil, the larger the mutual inductance M_{pr} becomes. Conversely, the closer the receiver coil is to the active coil, the larger the mutual inductance M_{arn} becomes. Compared with the traditional DWPT system, the proposed system employs a structure based on the repeater coil rather than powering all coils at the transmitter side. The repeater coil is powered by adjacent active coils on the left and right sides. During the movement of the receiver coil, the active coil and the repeater coil alternately serve as the main channel for power transfer.

B. Modeling of the Proposed System

To clarify the working principle of the proposed DWPT system, a DWPT system unit is shown in Fig. 2. The DWPT system unit consists of four coils: two active coils, one repeater coil, and one receiver coil. The active coil employs an LCL-compensated resonant structure, while both the repeater coil and receiver coil utilize series resonant structures. The self-inductances of the active coil, repeater coil, and receiver coil are denoted as L_{aci} (where $i = 1,2$), L_{rp}, and L_{re}, respectively, with the relationship $L_{Ti} = L_{aci} = L_{rp} = L$. The parameters of each component must satisfy the following conditions:

$$\begin{cases} \omega L_{Ti} = \frac{1}{\omega C_{\text{aci}}} = \omega L_{\text{aci}} \\ \omega L_{re} = \frac{1}{\omega C_{re}} \end{cases} \tag{1}$$

where ω is the angular frequency.

When the compensation network of the active coil satisfies the resonance conditions, the current flowing into the active coil remains constant. Therefore, the primary structure can be approximated as a constant current source [21]. The current can be calculated as follows:

$$I_{\text{aci}} = \frac{V}{j\omega L_{\text{aci}}} \tag{2}$$

where $V = 2\sqrt{2}V_{\text{in}}/\pi$, V_{in} is the input dc voltage.

R is the equivalent load of the rectifier on the receiver side, and the relationship between R and R_o is expressed as follows [22]:

$$R = \frac{8R_o}{\pi^2}. \tag{3}$$

The repeater coil in the proposed system is influenced by the magnetic induction from the left and right active coils. Since the relative positions between the repeater coil and the active coils remain unchanged, the induced voltage on the repeater coil remains constant. For simplicity, the parasitic resistance of each component in the system is neglected. Based on Kirchhoff's voltage law, the voltage loop equation for the proposed DWPT system is given as follows:

$$\begin{cases} j\omega M_{pr} I_{re} + 2j\omega M_{ap} I_{\text{ac1}} - j(\omega L_{rp} - \frac{1}{\omega C_{rp}}) I_{rp} = 0 \\ j\omega M_{ar1} I_{\text{ac1}} + j\omega M_{pr} I_{rp} - I_{re} R = 0. \end{cases} \tag{4}$$

The output power of the system is expressed as

$$P_{\text{out}} = |V_{re}||I_{re}| \cos\theta \tag{5}$$

where V_{re} is the voltage on the load, and θ is the phase angle difference between V_{re} and I_{re}.

C. Power Loss and Efficiency of the System

The system structure is shown in Fig. 3. The system's power loss primarily results from the passive components and switches. The loss in passive components is due to their parasitic resistance. The total losses in the passive components can be expressed as

$$P_{pas} = \sum_n I_{pn}^2 r_T + \sum_n I_{acn}^2 r_a + I_{rp}^2 r_p + I_{re}^2 r_e \tag{6}$$

where the subscript n represents the different active coils, and $n = 12$, r_T represents the parasitic resistance of L_{T1} and L_{T2}, r_a is the parasitic resistance of L_{ac1} and L_{ac2}, r_p is the parasitic resistance of L_{rp}, and r_e is the parasitic resistance of L_{re}.

The power loss of the switches includes conduction loss P_{con} and switching loss P_{sw} [23]. Assuming that all MOSFETs in the system have the same specifications, the conduction loss of the switch can be deduced as

$$P_{con} = \frac{1}{T} \int (2i_{ab}^2(t) + 2i_{p1}^2(t) + 2i_{p2}^2(t)) R_{on} dt \tag{7}$$

where T is the period of the switches, i_{ab} is the current flowing into the switches of the switch-controlled capacitor, i_{p1} and i_{p2} are the output currents of the inverter, and R_{ON} is the ON-resistance of the switches.

The SCC enables zero-voltage switching (ZVS) for both turn-ON and turn-OFF [24], which allows the switching loss of the SCC to be neglected. Therefore, the system's switching loss can be expressed as

$$\begin{cases} P_{\text{on}} = 2N_{HS\_\text{on}} f C_{ds} V_{\text{in}}^2 \\ P_{\text{off}} = N_{HS\_\text{off}} f V_{\text{in}} I_{\text{off}} (\frac{t_r}{3} + \frac{t_f}{2}) \\ P_{sw} = P_{\text{on}} + P_{\text{off}} \end{cases} \tag{8}$$

where N_{HS_ON} is the number of switches operating in hard turn-ON, N_{HS_OFF} is the number of switches operating in hard turn-OFF, f is the corresponding frequency of T, C_{ds} is the MOSFETs' drain-source capacitance, I_{OFF} is the turn-OFF current of the switches, t_r is the current rise time of the MOSFETs, and t_f is the current fall time of the MOSFETs.

Therefore, the total power loss of the system can be expressed as

$$P_{\text{loss}} = P_{pas} + P_{con} + P_{sw}. \tag{9}$$

Hence, the efficiency of the system can be expressed as

$$\eta = \frac{P_{\text{out}}}{P_{\text{out}} + P_{\text{loss}}}. \tag{10}$$

D. Power Transmission Performance at Different Positions

1) APR Mode: When the receiver coil is positioned in Region II, situated between the repeater coil and the active coil, the system operates in APR mode. This is the most common operating mode of the DWPT system and represents the transition from AR mode to PR mode, during which the primary power transfer channel shifts from the active coil to the repeater coil. In this mode, the mutual inductance between the active coil, repeater coil, and receiver coil cannot be ignored. The receiver coil simultaneously receives power from both the active coil and the repeater coil. The equivalent circuit of the system is shown in Fig. 3. In APR mode, the mutual inductances M_{ac1} and M_{pr} continuously vary, leading to significant power fluctuations. As the receiver coil moves closer to the repeater coil, M_{pr} gradually increases, while M_{ac1} gradually decreases. Conversely, as the receiver coil approaches the active coil, M_{ac1} increases and M_{pr} decreases. Therefore, by combining (2), (4), and (5), the current and power of the proposed DWPT system can be derived as

$$\begin{cases} I_{re} = \frac{V L_{rp}(M_{ar1}(\omega^2 C_{rp} L_{rp} - 1) + 2\omega^2 M_{ap} M_{pr} C_{rp})}{L_{\text{ac1}}(R L_{rp}(\omega^2 C_{rp} L_{rp} - 1) - j\omega^3 L_{rp} M_{pr}^2 C_{rp})} \\ I_{rp} = \frac{\omega V L_{rp} C_{rp}(\omega M_{ar1} M_{pr} - j2RM_{ap})}{L_{\text{ac1}}(R L_{rp}(\omega^2 L_{rp} C_{rp} - 1) - j\omega^3 L_{rp} M_{pr}^2 C_{rp})} \\ P_{\text{out}} = \frac{V^2 R((\omega^2 L_{rp}^2 C_{rp} - L_{rp}) M_{ar1} + 2\omega^2 L_{rp} C_{rp} M_{ap} M_{pr})^2}{L_{\text{ac1}}^2 (R^2 L_{rp}^2 (\omega^2 L_{rp} C_{rp} - 1)^2 + \omega^6 L_{rp}^2 C_{rp}^2 M_{pr}^4)}. \end{cases} \tag{11}$$

As indicated in (11), adjusting C_{rp} can control the current of the receiver coil and repeater coil, as well as the system's output power.

2) AR Mode: When the receiver coil is in Region I, aligned with the active coil, the system operates in AR mode. Due to the large distance between the repeater coil and the receiver coil, it can be assumed that $M_{pr} = 0$. The equivalent circuit of the system is shown in Fig. 4. Consequently, the current and power of the proposed DWPT system can be expressed as

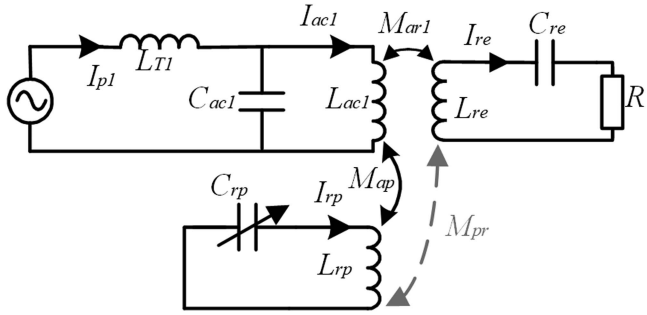

Fig. 4. Equivalent circuit of the DWPT system in AR mode.

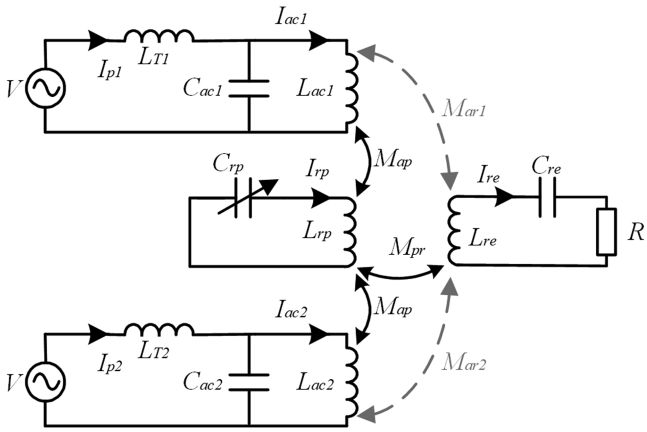

Fig. 5. Equivalent circuit of the DWPT system in PR mode.

$$\begin{cases} I_{re} = \frac{V M_{ar1}}{L_{\text{ac1}} R} \\ I_{rp} = \frac{-j2\omega^2 V R L_{rp} C_{rp} M_{ap}}{\omega R(\omega^2 L_{rp} C_{rp} - 1) L_{\text{ac1}} L_{rp}} \\ P_{\text{out}} = \frac{V^2 M_{ar1}^2}{R L_{\text{ac1}}^2}. \end{cases} \tag{12}$$

As indicated in (12), adjusting the capacitance C_{rp} allows for control of the current in the repeater coil. However, in this mode, the output power P_{out} is solely determined by the load R, the self-inductance L_{ac1}, and mutual inductance M_{ac1}.

3) PR Mode: When the receiver coil is in Region III, aligned with the repeater coil, the system operates in PR mode. Due to the large distance between the active coil and the receiver coil, it can be assumed that $M_{\text{ac1}} = 0$. The equivalent circuit of the system is shown in Fig. 5. Consequently, the current and power of the proposed DWPT system can be expressed as follows:

$$\begin{cases} I_{re} = \frac{2\omega^2 V L_{rp} C_{rp} M_{ap} M_{pr}}{L_{\text{ac1}}(R L_{rp}(\omega^2 C_{rp} L_{rp} - 1) - j\omega^3 L_{rp} M_{pr}^2 C_{rp})} \\ I_{rp} = \frac{-j2R\omega V L_{rp} C_{rp} M_{ap}}{L_{\text{ac1}}(R L_{rp}(\omega^2 L_{rp} C_{rp} - 1) - j\omega^3 L_{rp} M_{pr}^2 C_{rp})} \\ P_{\text{out}} = \frac{4V^2 R L_{rp}^2 C_{rp}^2 M_{ap}^2 M_{pr}^2}{L_{\text{ac1}}^2 (R^2 L_{rp}^2 (\omega^2 L_{rp} C_{rp} - 1)^2 + \omega^6 L_{rp}^2 C_{rp}^2 M_{pr}^4)}. \end{cases} \tag{13}$$

As indicated in (13), in PR mode, the repeater coil serves as the main power transmission channel, delivering power to the receiver coil. In this mode, adjusting the capacitance C_{rp}

allows for control of both the current in the repeater coil and the receiver coil. Additionally, the output power is dependent on the capacitance C_{rp}.

III. Control Strategy Based on Detuning Rate

A. Definition and Control Method of Detuning Rate

In an ideal state, when the receiver coil is positioned directly above the active coil, $M_{pr} = 0$.

Assuming that the repeater coil unit is in a resonant state, the current in the repeater coil would approach infinity, which greatly endangers the safety of the system. Therefore, to suppress the no-load current of the repeater coil, the repeater coil of the proposed DWPT system is designed to be in a detuned state. The imaginary impedance of the repeater coil loop is given by

$$X_{rp} = \omega L_{rp} - \frac{1}{\omega C_{rp}}. \tag{14}$$

The detuning rate is introduced to characterize the strength of the detuning effect of the repeater coil, which is defined as the numerical ratio of the imaginary impedance of the repeater coil loop to the inductance of the repeater coil. The expression is as follows:

$$\alpha = \frac{X_{rp}}{\omega L_{rp}}. \tag{15}$$

Substituting (14) and (15) into (11), the current in the repeater coil, the current in the receiver coil, and output power can be obtained as

$$\begin{cases} I_{re} = \frac{V(\alpha L_{rp} M_{ar1} + 2M_{ap} M_{pr})}{L_{ac1}(\alpha L_{rp} R - j\omega M_{pr}^2)} \\ I_{rp} = \frac{V(\omega M_{ar1} M_{pr} - j2RM_{ap})}{\omega L_{ac1}(\alpha L_{rp} R - j\omega M_{pr}^2)} \\ P_{\text{out}} = \frac{V^2 R(\alpha L_{rp} M_{ar1} + 2M_{ap} M_{pr})^2}{L_{ac1}^2(\alpha^2 L_{rp}^2 R^2 + \omega^2 M_{pr}^4)}. \end{cases} \tag{16}$$

As indicated in (16), when the mutual inductance between the repeater coil and the receiver coil is particularly small, increasing the detuning rate can suppress the current in the repeater coil, reduce its no-load loss, and adjust the current in the repeater coil and the output power by adjusting the detuning rate of the repeater coil.

A SCC is introduced to control the detuning rate of the repeater coil. By controlling the switch drive signal of the switch-controlled capacitor, the duration for which the capacitor is passed and bypassed can be varied, thereby modifying the equivalent capacitance value of the switch-controlled capacitor. The structure and typical waveform of the SCC are shown in Fig. 6, where β is the phase shift angle of the switch drive signal. The structure of the SCC is shown in Fig. 6(a), which consists of two switches connected in series and a capacitor connected in parallel.

The voltage u_{ab} at both terminals A and B is shown in Fig. 6(b). When the switches S_a and S_b are turned ON and OFF, u_{ab} remains at 0, enabling ZVS during both turn-ON and turn-OFF. Furthermore, once the switches S_a and S_b are turned ON, their antiparallel diodes become reverse-biased, thereby minimizing the impact of the reverse recovery current.

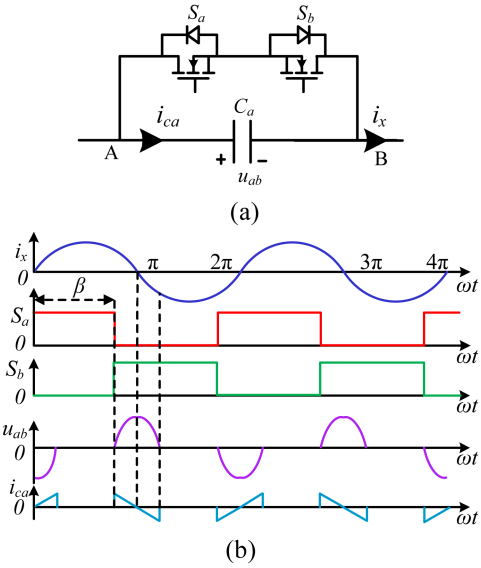

Fig. 6. Switch-controlled capacitor. (a) Structure. (b) Typical waveforms.

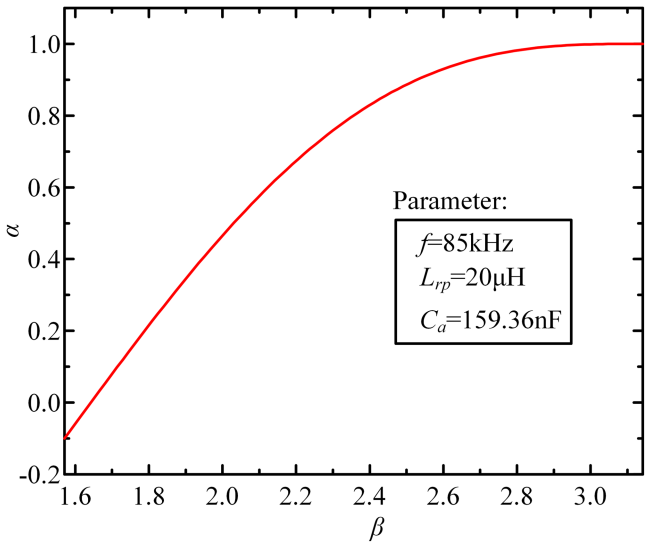

Fig. 7. Detuning rate α versus phase angle shift β.

The equivalent capacitance value of the SCC can be expressed as [25], [26]

$$C_{sc} = \frac{\pi C_a}{2\pi - 2\beta + \sin 2\beta}. \tag{17}$$

The detuning rate of the repeater coil as a function of the phase shift angle β is shown in Fig. 7. Clearly, the detuning rate of the repeater coil can be effectively adjusted by varying the phase shift angle. When $\beta = \pi/2$, the detuning rate is at its minimum, indicating capacitive detuning. When $\beta = 1.63\pi$, $\alpha = 0$, indicating that the repeater coil is in a resonant state. When $\beta = \pi$, $\alpha = 1$, and the equivalent capacitance approaches infinity, it is equivalent to a short circuit. The detuning rate increases with the phase shift angle. When the system is in inductive detuning, a higher detuning rate results in increased impedance in the repeater coil, which reduces the current and limits the power

output capability. Therefore, as the phase shift angle decreases, the power output capability of the repeater coil increases.

B. Detuning Rate Control Strategy

As the receiver coil transitions from the active coil to the repeater coil, the repeater coil gradually serves as the primary power supply. The power output capability of the repeater coil differs from that of the active coil. Therefore, it is essential to control the detuning rate of the repeater coil to ensure constant power output and safe system operation, while also limiting the current in the repeater coil.

As seen in (12), when the system operates in AR mode, the output power is unaffected by the detuning rate of the repeater coil and is solely determined by the mutual inductance M_{ac1} and the load R. Therefore, when the load of the DWPT system is fixed, the output power in AR mode remains constant. To ensure a constant output power, the power output of the system should be set to $P_{\mathrm{AR.out}}$. In this mode, the repeater coil operates under no-load conditions. Consequently, it is essential to adjust the detuning rate of the repeater coil to its maximum to minimize the current in the repeater coil, reduce no-load losses, and improve the system's efficiency. The system's constant power output is given by

$$P^{*}_{\mathrm{out}} = P_{\mathrm{AR.out}} = \frac{V^2 M^2_{ar1.\mathrm{AR}}}{R L^2_{\mathrm{ac1}}} \tag{18}$$

where $M_{ar1.\mathrm{AR}}$ represents the mutual inductance between the active coil and the receiver coil in AR mode, and $P*$ out is the constant output power.

When the system operates in PR mode, the repeater coil becomes the primary power transmission channel. The output power of the system is rewritten as

$$P_{\mathrm{PR.out}} = \frac{4V^2 R M^2_{ap} M^2_{pr}}{L^2_{\mathrm{ac1}}(\alpha^2 L^2_{rp} R^2 + \omega^2 M^4_{pr})}. \tag{19}$$

The variation of the system's output power in PR mode with respect to the detuning rate α is shown in Fig. 8. As illustrated in Fig. 8, as the detuning rate of the repeater coil increases, the system's output power first increases and then decreases. When $\alpha = 0$, the output power of the repeater coil reaches its maximum. The maximum output power can be expressed as

$$P_{\mathrm{PR.out\_max}} = \frac{4V^2 R M^2_{ap}}{\omega^2 L^2_{\mathrm{ac1}} M^2_{pr}}. \tag{20}$$

The system parameters used in this section are shown in Table I. Fig. 9 illustrates the impact of the detuning rate α on P_{out} during the dynamic process. As the detuning rate α increases, the system's output power correspondingly decreases. When the detuning rate of the repeater coil is fixed, the system cannot maintain a constant power output, resulting in significant power fluctuations. Fig. 9 shows that the expected constant power curve always intersects with the system's output power curve. When the receiver coil remains in the same position, a smaller detuning rate results in higher output power. Excluding the output power in AR mode, regardless of the offset distance, the output power curve intersects with the expected constant power curve at most

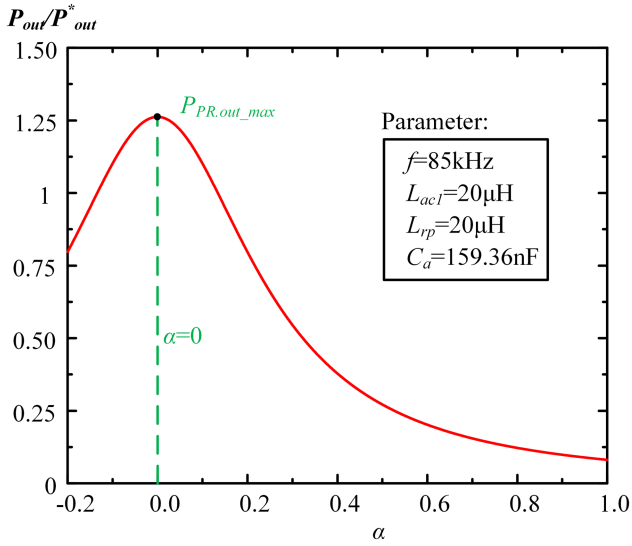

Fig. 8. Variation of the system's output power in PR mode against the detuning rate α.

TABLE I
SIMULATION PARAMETERS OF THE PROPOSED SYSTEM

Parameter	Value
L_{T1}&L_{ac1}&L_{rp}	20 μH
L_{re}	47 μH
C_{ac1}	175 nF
C_{re}	74.6 nF
M_{ap}	1.2 μH
R	20 Ω
V_{in}	60 V

once. Therefore, regardless of the receiver coil's position, there is a unique detuning rate that enables the output power at that position to be the rated output power. Therefore, achieving constant power output by real-time control of the repeater coil's detuning rate during the dynamic process is feasible.

The variation of output power P_{out} and detuning rate α against the offset distance, after incorporating a SCC in the repeater coil, are shown in Fig. 10. It demonstrates that as the receiver coil moves closer to the repeater coil and the detuning rate α decreases, the system's output power exhibits minimal fluctuation and remains nearly constant. Therefore, to achieve constant power output during the dynamic process, it is only necessary to ensure that the maximum output power in PR mode is greater than or equal to the output power in AR mode by controlling the detuning rate of the repeater coil.

When the system satisfies the condition for constant power output, the detuning rate α of the repeater coil can be expressed as

$$\alpha = \frac{2RV^2 M_{ap} M_{ar1} M_{pr} + \lambda}{R L_{rp}(P^{*}_{\mathrm{out}} R L^2_{\mathrm{ac1}} - V^2 M^2_{ar1})} \tag{21}$$

where

$$\lambda = \sqrt{P^{*}_{\mathrm{out}} R L^2_{\mathrm{ac1}} M^2_{pr}(4R^2V^2M^2_{ap} + \omega M^2_{pr}(V^2 M^2_{ar1} - P^{*}_{\mathrm{out}} R L^2_{\mathrm{ac1}}))}.$$

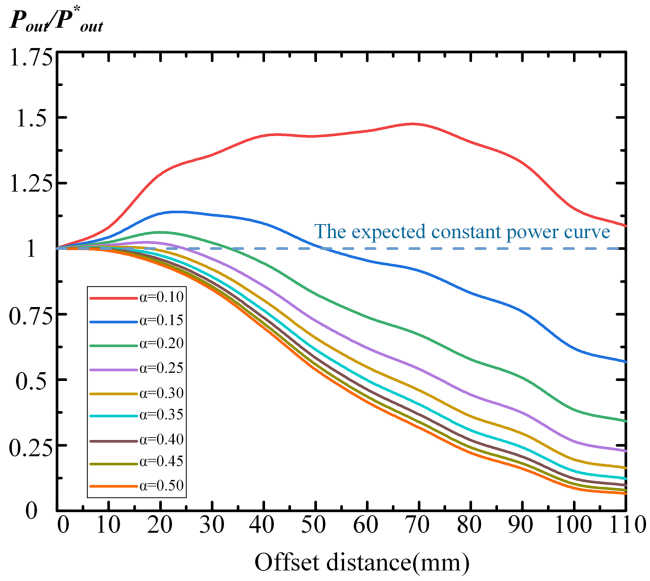

Fig. 9. $P_{\text{out}}/P^*_{\text{out}}$ variation against the offset distances. (the fixed-value capacitor).

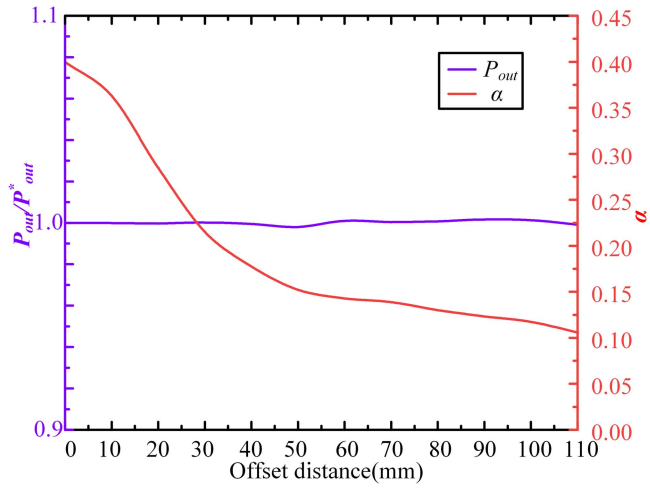

Fig. 10. $P_{\text{out}}/P^*_{\text{out}}$ and α variation against the offset distances (the switch-controlled capacitor).

C. Analysis of System Parameters Variations

1) M_{ap} Variation: According to (16), when the detuning rate α is constant, the output power varies in response to changes in the mutual inductance between the active coil and the repeater coil. The variations of the output power P_{out} and the detuning rate α under different M_{ap} in the proposed DWPT system are shown in Fig. 11. As illustrated, a larger M_{ap} corresponds to a higher detuning rate α. As the receiver coil moves closer to the repeater coil, the detuning rate consistently decreases, enabling the system to maintain a constant power output.

According to (20), the maximum output power in PR mode is proportional to M_{ap}^2. Consequently, as M_{ap} decreases, $P_{\text{PR.out\_max}}$ may fall below $P_{\text{AR.out}}$, which could prevent the system from maintaining a constant power output. To ensure constant power output, the system must satisfy the following

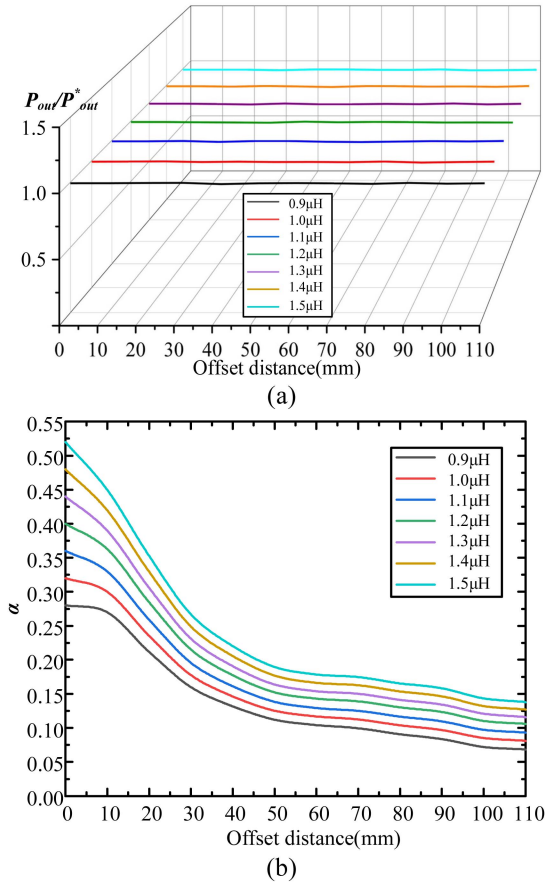

Fig. 11. $P_{\text{out}}/P^*_{\text{out}}$ and α Variation under different M_{ap}. (a) $P_{\text{out}}/P^*_{\text{out}}$. (b) α.

condition:

$$M_{ap} \geq \frac{\omega M_{pr.\text{PR}} M_{ar1.\text{AR}}}{2R} \tag{22}$$

where $M_{pr.\text{PR}}$ represents the mutual inductance between the repeater coil and the receiver coil in PR mode.

In conclusion, when the system parameters satisfy the conditions specified in (22), fluctuations in the output power caused by changes in the mutual inductance M_{ap} can be offset by controlling α.

2) R Variation: In practical applications, the equivalent load constantly varies during the charging process. Therefore, it is essential to evaluate the performance of the proposed system as the load changes. Based on (16), (18), and (19), the output voltage of the proposed system can be expressed as

$$\begin{cases} U_{\text{AR.out}} = \frac{VM_{ar1}}{L_{\text{ac1}}} \\ U_{\text{APR.out}} = \frac{VR(\alpha L_{rp} M_{ar1} + 2M_{ap} M_{pr})}{L_{\text{ac1}} \sqrt{(\alpha^2 L_{rp}^2 R^2 + \omega^2 M_{pr}^4)}} \\ U_{\text{PR.out}} = \frac{2VRM_{ap} M_{pr}}{L_{\text{ac1}} \sqrt{(\alpha^2 L_{rp}^2 R^2 + \omega^2 M_{pr}^4)}}. \end{cases} \tag{23}$$

According to (23), it can be inferred that the output voltage in AR mode is independent of the detuning rate. Therefore, the constant voltage of the system should be set to $U_{\text{AR.out}}$. By controlling the detuning rate of the repeater coil, the system can maintain a constant voltage output. The variation of the

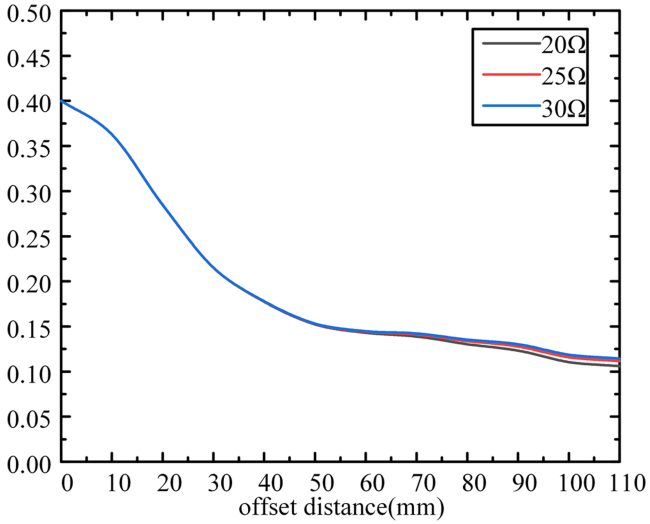

Fig. 12. α variation under different R.

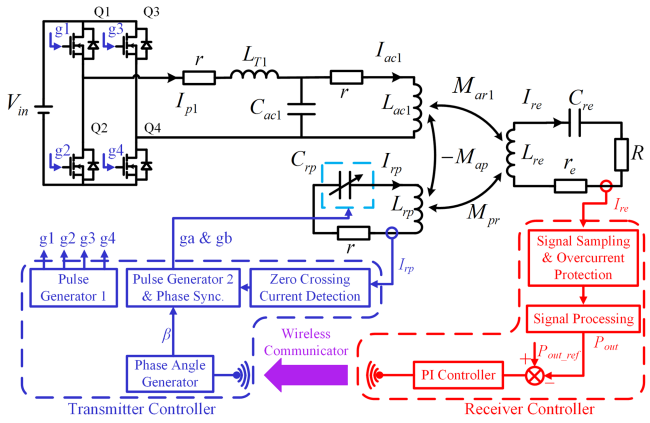

Fig. 13. Control block diagram of the proposed control strategy.

detuning rate required for maintaining a constant voltage output in the proposed DWPT system under different load conditions is shown in Fig. 12. As depicted, a larger resistance R corresponds to a higher detuning rate. As the receiver coil moves closer to the repeater coil, the detuning rate decreases, enabling the system to maintain a constant voltage output.

The conditions for achieving constant voltage output in the system can be derived as follows:

$$R \geq \frac{\omega M_{pr.\mathrm{PR}} M_{ar1.\mathrm{AR}}}{2M_{ap}}. \tag{24}$$

In conclusion, when the system parameters satisfy the conditions specified in (24), fluctuations in the output voltage caused by changes in load R M_{ap} can be offset by controlling α.

D. Control Block Diagram

The control block diagram is shown in Fig. 13. The output current Ire is initially sampled and processed through a signal processing circuit to calculate the output power Pout. The output power error is fed to the PI controller to adjust the phase shift angle β of the driving signal for the switch-controlled capacitor. This phase angle information is transmitted to the transmitter controller via a wireless communicator. The transmitter controller continuously samples the current in the repeater coil and uses a zero-crossing current detector to generate a square wave synchronized with the zero-crossing signals. The pulse generator then combines this zero-crossing signal with the phase angle signal β, producing a driving signal for the SCC refer to Fig. 6.

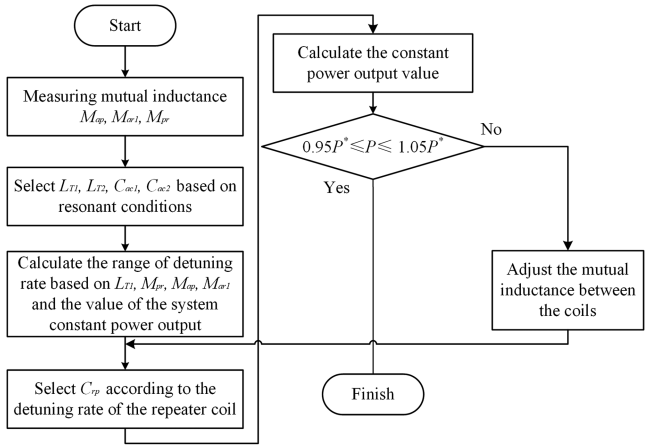

Fig. 14. Flowchart of the proposed DWPT system.

As illustrated in Fig. 9, the system's output power increases as the detuning rate decreases. Therefore, a unique detuning rate exists for each position of the receiver coil that enables the system to achieve the desired output power. According to Fig. 14, the sampled current is used to calculate the output power, which serves as a feedback signal. The initial phase angle is set to its maximum value to ensure system safety. Based on the output power of the receiver coil, the power error is calculated and fed to the PI controller to generate the corresponding control signal. This signal adjusts the phase shift angle according to the control signal.

E. Parameter Design Consideration

To clearly explain how to design the parameters of the proposed DWPT system, the flow chart is shown in Fig. 14. The detailed design procedures are as follows.

1) Measuring mutual inductance M_{ap}, M_{ar1}, M_{pr}.
2) Select L_{T1}, L_{T2}, C_{ac1}, C_{ac2} based on (1).
3) Calculate the range of the detuning rate based on L_{T1}, M_{pr}, M_{ap}, M_{ar1}, and the value of the system constant power output based on (18).
4) Select C_{rp} according to the detuning rate of the repeater coil.
5) Calculate the constant power output value P.
6) Determine whether $0.95P^* \leq P \leq 1.05P^*$. If yes, the design is finished. If not, go to step (7).
7) Adjust the mutual inductance between the coils. Then, go to step (4).

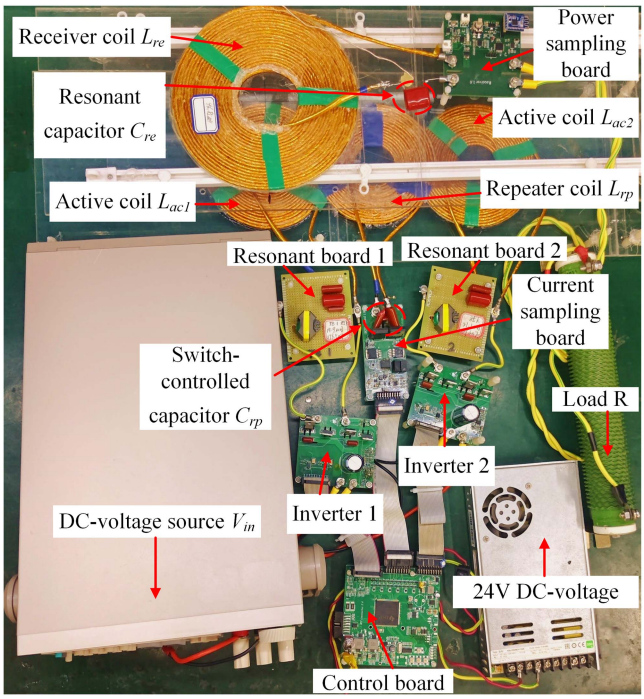

Fig. 15. Experimental prototype of the proposed DWPT system.

IV. Experimental Verification

A. Experiment Set Up

To verify the feasibility of the proposed DWPT system, an experimental prototype was constructed, as shown in Fig. 15. The specifications of the experimental prototype are as follows: Dc voltage $V_{\text{in}} = 60$ V, output voltage $V_o = 23$ V, rated output power $P_o = 27$ W, and operating frequency $f_s = 85$ kHz. The experimental prototype includes a dc voltage source, a control board, two inverter boards, two resonant boards, a SCC control board, a power sampling board, and a load resistor. The core component of the control board is a DSP controller of TMS320F28335, which handles signal processing, algorithm implementation, communication, ADC sampling, and other functions. In this system, the control board generates an 85 kHz PWM signal to control the inverter switches, samples the zero-crossing point of the repeater coil, calculates the output power, and outputs the corresponding drive signals to control the switch of the repeater coil's switch-controlled capacitor. A full-bridge inverter, composed of four MOSFETs of FDP51N25, is used to generate a square wave voltage and is driven by the gate drivers of IR2113STRPBF. Two MOSFETs of GC3M0060065K are connected in parallel with a capacitor to form the SCC and are driven by the gate drivers of SI8233BB-D-IS. The component parameters of the experimental prototype are measured using the Tonghui precision LCR tester TH2827C, and the results are shown in Table II.

B. Experimental Results

Fig. 16 presents the output waveforms of the system during the whole dynamic process, along with the zoomed-in waveforms and the corresponding typical waveforms of the SCC in three different modes. Fig. 16(b), (c), and (d), respectively, shows the output voltage of the inverter and the current in different coils in AR mode, APR mode, and PR mode. Fig. 16(e), (f), and (g) shows the phase shift angle and the voltage of the SCC in AR mode, APR mode, and PR mode, corresponding to Fig. 16(b), (c), and (d), respectively. V_{in} is the output voltage of the inverter, I_{ac1} is the current of the active coil 1, I_{rp} is the current of the repeater coil, and I_{re} is the output current, V_{g_S1} is the driving signal of the switch S_1 of the switch-controlled capacitor, and u_{Crp} is the voltage of the switch-controlled capacitor. In Fig. 16(b), compared to the other two modes, I_{rp} is the smallest, with an rms value of 3.44 A. In AR mode, the repeater coil operates in an unloaded state, at which point the impedance of the repeater coil is at its maximum. This helps limit the current in the repeater coil, ensuring the system's safety. Additionally, I_{ac1} and I_{rp} are nearly in phase, indicating that the power received by the receiver coil is the sum of the output power from both the repeater coil and the active coil. As the receiver coil moves from the active coil to the repeater coil, the current in the repeater coil gradually increases from 3.44 A in AR mode to 4.88 A in PR mode. In Fig. 16(e), when the system is in AR mode, the phase shift angle of the switch drive signal is the largest, at 0.63π. In Fig. 16(g), when the system is in PR mode, the phase shift angle is the smallest, at 0.57π. The increase in the current of the repeater coil and the decrease in the phase shift angle of the SCC (the decrease in detuning rate) are aimed at enhancing the power output capacity of the repeater coil, thereby ensuring constant power output and improving the system's efficiency. As illustrated in Fig. 16(a), during the whole dynamic process, I_{ac1} remains constant, while I_{rp} gradually increases to a peak and then decreases. I_{re} remains nearly constant throughout the movement, with minimal fluctuations in the output power. This demonstrates that the proposed DWPT system maintains constant power output during the whole dynamic process. Moreover, the current waveforms of I_{re} and I_{rp} exhibit symmetry throughout the movement, indicating that the system's output characteristics are fully symmetrical as the receiver coil moves from active coil 1 to the repeater coil, and then from the repeater coil to active coil 2.

The SCC not only adjusts the detuning rate of the repeater coil but also enables ZVS for the switches. When S_1 is turned ON

TABLE II
Parameters of the Experimental Prototype

Parameter	Value
L_{T1}	20.45 μH
L_{T2}	20.38 μH
C_{ac1}	174.5 nF
C_{ac2}	173.7 nF
L_{ac1}	19.74 μH
L_{ac2}	20.7 μH
L_{rp}	21.3 μH
L_{re}	46.85 μH
C_{rp}	146.78 nF
M_{ap}	1.21 μH
R	20.03 Ω
V_{in}	60 V

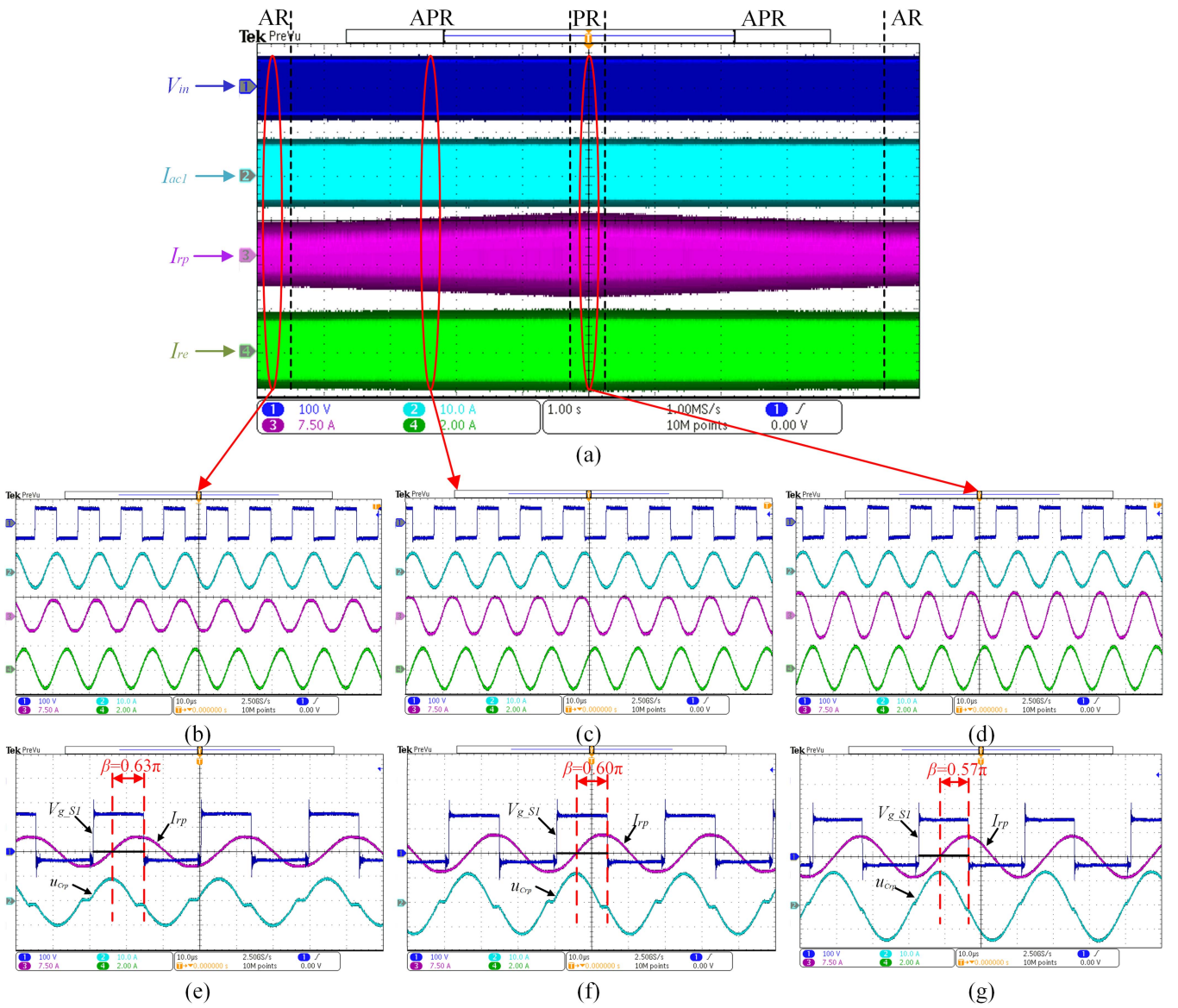

Fig. 16. Waveforms of the whole dynamic process, zoomed-in waveforms and the typical waveforms of the SCC in three different modes. (a) Whole process; and detail waveforms of inverter output voltage and current in different coils: (b) AR mode; (c) APR mode; (d) PR mode; and phase shift angle and voltage of the SCC in (e) AR mode; (f) APR mode; (g) PR mode.

and S_2 is turned OFF, the capacitor charges, causing the voltage across it to increase. As the current in the repeater coil shifts from positive to negative, the capacitor discharges, leading to a decrease in the voltage. Once the charging and discharging cycle is complete, S_1 turns OFF and S_2 turns ON. This process allows both switches of the SCC to achieve ZVS. As shown in Fig. 16(e), (f), and (g), both switches of the capacitor successfully achieve ZVS.

Fig. 17 presents the simulation and experimental results for the output power, efficiency, and phase shift angle against the offset distance. As illustrated in Fig. 17, by adjusting the detuning rate of the repeater coil, the output power remains constant at around 27 W, with fluctuations of less than 5% throughout the entire movement. In AR mode, the system's highest efficiency is 89%, while in PR mode, the lowest efficiency is 81%. The experimental and simulation results are in good agreement, confirming the accuracy of the theoretical modeling and analysis.

C. Experimental Results Under Different Parameters

Fig. 18 illustrates the system's output power and phase shift angle under varying mutual inductance conditions. In AR mode, the output power remains constant, unaffected by variations in mutual inductance. As the mutual inductance between the repeater coil and the active coil increases, the detuning rate at each position correspondingly increases. Furthermore, as the receiver coil moves closer to the repeater coil, a decreasing trend in the detuning rate is observed.

Fig. 19 shows the system's output voltage under different load conditions. As illustrated, a constant output voltage of

TABLE III
COMPARISON BETWEEN THE PROPOSED SYSTEM AND RELATED REFERENCES

Reference	Transmitter Coil Diameter / Receiver Movement Distance	Operation Frequency	Rated Power	Number of Active Coils	Number of Inverters	Primary Compensation Networks	Minimum Efficiency	Maximum Power Fluctuation	Constant profile transfer under Varying Mutual Inductance
[19]	154mm / 161.5mm	80kHz	150W	N	N	N*LCL	<10%	Discontinuous power transfer	/
[20]	230mm / 250mm	85kHz	766W	N	N	3N*C+2N*L	<60%	Discontinuous power transfer	/
[22]	350mm / 100mm	85kHz	3.3kW	N	N	N*LCL+N*LC	93%	9.1%	NO
[23]	130mm / 110mm	85kHz	100W	N/2	N/2	N/2*LCL+N/2*LC	79%	8.5%	NO
This work	**130mm / 100~120mm**	**85kHz**	**27W**	**N/2**	**N/2**	**N/2*LCL+N/2*LC**	**81%**	**4.8%**	**0.75~1.25 M_{ap}**

Note: The "/" indicates that the reference does not mention it, or the system cannot achieve constant power transfer.

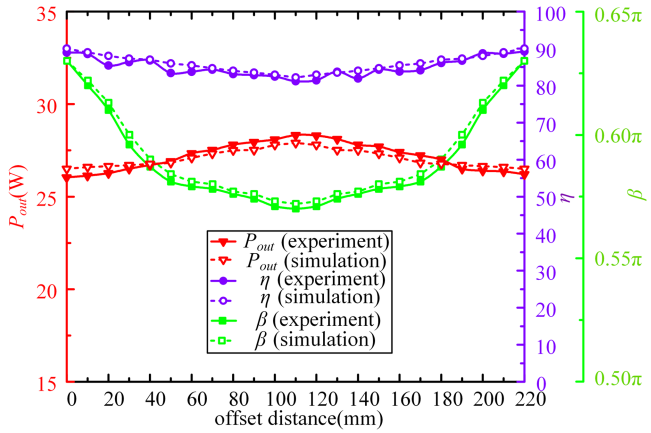

Fig. 17. Output power, efficiency, and phase shift angle variations against offset distance.

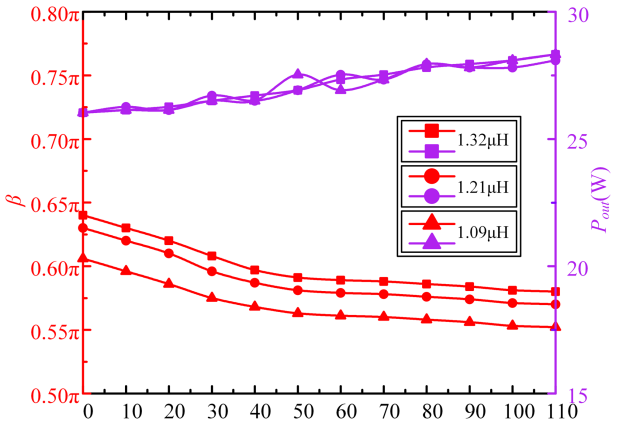

Fig. 18. System's output power P_{out} and phase shift angle β under different mutual inductance conditions.

23 V is maintained under different load conditions, with voltage fluctuations of less than 5%.

D. Comparison and Discussion

To intuitively illustrate the performance of the proposed system, Table III presents a comparison of the performance of

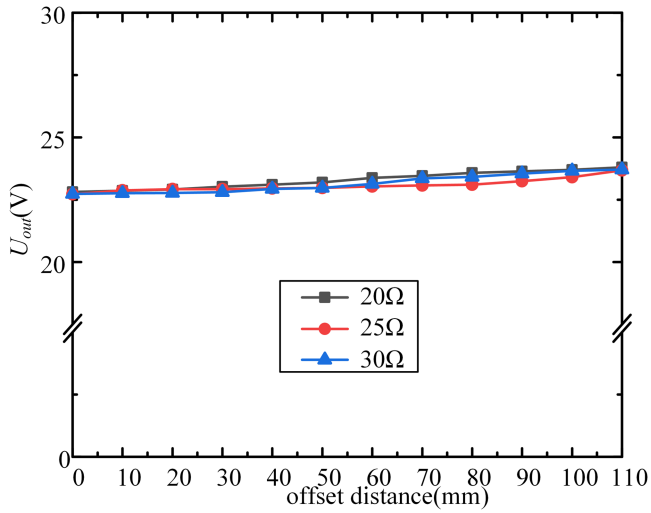

Fig. 19. System's output voltage U_{out} under different load conditions.

the existing DWPT systems. In [16] and [17], although these systems can achieve dynamic charging, their low efficiency combined with the inability to sustain continuous power transfer, presents a significant limitation. In [19], while the use of a three-resonator topology improves the efficiency of the system, it also complicates the system and increases the installation costs. Compared to [20], which also employs a repeater coil structure, the proposed system demonstrates higher efficiency and lower power fluctuations, maintaining a constant power output even when mutual inductance between the repeater coil and the active coil varies. Overall, considering these performance factors, the proposed DWPT system exhibits superior overall performance.

V. CONCLUSION

This article proposes a DWPT system with a controllable detuning rate that ensures constant power output throughout the dynamic process. By adjusting the equivalent capacitance of the switch-controlled capacitor, the impedance of the repeater coil can be modified, enhancing the system's control flexibility and improving efficiency. In a no-load state, the impedance of the repeater coil is increased to suppress the no-load current and

minimize losses. As the receiver coil approaches the repeater coil, the detuning rate of the repeater coil is reduced to enhance its power output capability, ensuring constant power output. A 27 W experimental prototype was developed based on the proposed optimization design method, confirming the feasibility and effectiveness of the DWPT system. The experimental results demonstrate that the system maintains constant power output throughout the entire dynamic process, with a maximum power fluctuation of 4.8% and an efficiency of approximately 85%. Moreover, the system can maintain constant power output under different mutual inductance conditions.

REFERENCES

[1] Y. Yao, S. Gao, Y. Wang, X. Liu, X. Zhang, and D. Xu, "Design and optimization of an electric vehicle wireless charging system using interleaved boost converter and flat solenoid coupler," *IEEE Trans. Power Electron.*, vol. 36, no. 4, pp. 3894–3908, Apr. 2021.

[2] Z. Luo, S. Nie, M. Pathmanathan, and P. W. Lehn, "Exciter–quadrature–repeater transmitter for wireless electric vehicle charging with high lateral misalignment tolerance and low EMF emission," *IEEE Trans. Transp. Electrific.*, vol. 7, no. 4, pp. 2156–2167, Dec. 2021.

[3] C. Jiang, K. T. Chau, W. Liu, C. Liu, W. Han, and W. H. Lam, "An LCC-compensated multiple-frequency wireless motor system," *IEEE Trans. Ind. Inform.*, vol. 15, no. 11, pp. 6023–6034, Nov. 2019.

[4] H. Li, L. Tan, H. Xu, Z. Wu, and X. Huang, "A wide-range global optimal control strategy for wireless charging systems in electric vehicles," *IEEE Trans. Power Electron.*, vol. 39, no. 12, pp. 16864–16876, Dec. 2024.

[5] E. S. Lee, B. H. Choi, Y. H. Sohn, G. C. Lim, and C. T. Rim, "Multiple dipole receiving coils for 2-D omnidirectional wireless mobile charging under wireless power zone," in *Proc. IEEE Energy Convers. Congr. Expo.*, 2015, pp. 3209–3214.

[6] P. Y. Wang, L. Sang, and K. Wang, "Optimization of simultaneous wireless power and data transmission system with single coil," in *Proc. Int. Conf. Power Electron. Syst. Appl.*, 2020, pp. 1–6.

[7] M. R. Basar, M. Y. Ahmad, J. Cho, and F. Ibrahim, "An improved wearable resonant wireless power transfer system for biomedical capsule endoscope," *IEEE Trans. Ind. Electron.*, vol. 65, no. 10, pp. 7772–7781, Oct. 2018.

[8] D. Patil, M. K. McDonough, J. M. Miller, B. Fahimi, and P. T. Balsara, "Wireless power transfer for vehicular applications: Overview and challenges," *IEEE Trans. Transp. Electrific.*, vol. 4, no. 1, pp. 3–37, Mar. 2018.

[9] A. C. Bagchi, A. Kamineni, R. A. Zane, and R. Carlson, "Review and comparative analysis of topologies and control methods in dynamic wireless charging of electric vehicles," *IEEE J. Emerg. Sel. Topics Power Electron.*, vol. 9, no. 4, pp. 4947–4962, Aug. 2021.

[10] G. Buja, M. Bertoluzzo, and H. K. Dashora, "Lumped track layout design for dynamic wireless charging of electric vehicles," *IEEE Trans. Ind. Electron.*, vol. 63, no. 10, pp. 6631–6640, Oct. 2016.

[11] K. Kim, J. Kim, H. Kim, J. Ahn, H. H. Park, and S. Ahn, "Evaluation of electromagnetic field radiation from wireless power transfer electric vehicle," in *Proc. Int. Symp. Antennas Propag.*, 2016, pp. 40–41.

[12] Z. Zhang, H. Pang, A. Georgiadis, and C. Cecati, "Wireless power transfer—An overview," *IEEE Trans. Ind. Electron.*, vol. 66, no. 2, pp. 1044–1058, Feb. 2019.

[13] H. Xu, Z. Huang, X. L. Li, and C. K. Tse, "Misalignment-tolerant IPT coupler with enhanced magnetic flux variation suppression and reduced copper usage," *IEEE Trans. Power Electron.*, vol. 39, no. 8, pp. 10506–10517, Aug. 2024.

[14] K. Wu, Y. Wang, X. Liu, J. Mai, and D. Xu, "A novel high-misalignment tolerant magnetic coupler for IPT system with concentrated magnetic flux and counteracting coil," *IEEE Trans. Ind. Appl.*, vol. 60, no. 4, pp. 6339–6350, Jul./Aug. 2024.

[15] H. Xu, L. Tan, L. Gui, Z. Wu, H. Li, and X. Huang, "Design of magnetic coupler for wireless power transmission system based on magnetic field reconstruction," *IEEE Trans. Power Electron.*, vol. 39, no. 2, pp. 2855–2866, Feb. 2024.

[16] X. Dai, J.-C. Jiang, and J.-Q. Wu, "Charging area determining and power enhancement method for multiexcitation unit configuration of wirelessly dynamic charging EV system," *IEEE Trans. Ind. Electron.*, vol. 66, no. 5, pp. 4086–4096, May 2019.

[17] S. Y. Jeong, J. H. Park, G. P. Hong, and C. T. Rim, "Autotuning control system by variation of self-inductance for dynamic wireless EV charging with small air gap," *IEEE Trans. Power Electron.*, vol. 34, no. 6, pp. 5165–5174, Jun. 2019.

[18] X. Mao, J. Chen, Y. Zhang, and J. Dong, "A simple and reconfigurable wireless power transfer system with constant voltage and constant current charging," *IEEE Trans. Power Electron.*, vol. 37, no. 5, pp. 4921–4925, May 2022.

[19] Y. Yao, A. U. Ibrahim, and W. Zhong, "A three-resonator wireless power transfer system with constant-output feature within a misalignment range," *IEEE Trans. Power Electron.*, vol. 37, no. 12, pp. 15753–15763, Dec. 2022.

[20] W. Xiong, Q. Yu, Z. Liu, L. Zhao, Q. Zhu, and M. Su, "A detuning-repeater-based dynamic wireless charging system with quasi-constant output power and reduced inverter count," *IEEE Trans. Power Electron.*, vol. 38, no. 1, pp. 1336–1347, Jan. 2023.

[21] Y. Yao, Y. Wang, X. Liu, F. Lin, and D. Xu, "A novel parameter tuning method for a double-sided LCL compensated WPT system with better comprehensive performance," *IEEE Trans. Power Electron.*, vol. 33, no. 10, pp. 8525–8536, Oct. 2018.

[22] Y. Huang, C. Liu, Y. Xiao, and S. Liu, "Separate power allocation and control method based on multiple power channels for wireless power transfer," *IEEE Trans. Power Electron.*, vol. 35, no. 9, pp. 9046–9056, Sep. 2020.

[23] M. K. Kazimierczuk and D. Czarkowski, "Class D series-resonant inverters," in *Resonant Power Converters*, 2nd ed. Hoboken, NJ, USA: Wiley, 2011.

[24] J. Zhang, J. Zhao, Y. Zhang, and F. Deng, "A wireless power transfer system with dual switch-controlled capacitors for efficiency optimization," *IEEE Trans. Power Electron.*, vol. 35, no. 6, pp. 6091–6101, Jun. 2020.

[25] D. Kim and D. Ahn, "Self-tuning LCC inverter using PWM-controlled switched capacitor for inductive wireless power transfer," *IEEE Trans. Ind. Electron.*, vol. 66, no. 5, pp. 3983–3992, May 2018.

[26] J. Osawa, T. Isobe, and H. Tadano, "Efficiency improvement of high frequency inverter for wireless power transfer system using a series reactive power compensator," in *Proc. IEEE 12th Int. Conf. Power Electron. Drive Syst.*, 2017, pp. 992–998.

Wenjing Xiong (Member, IEEE) was born in Hunan, China, in 1991. She received the B.S. degree in automation and the Ph.D. degree in control science and engineering from Central South University, Changsha, China, in 2012 and 2017, respectively.

She is currently an Associate Professor with the School of Automation, Central South University. Her research interests include modulation strategy for matrix converter and ac/dc converters, and wireless power transfer system.

Jiawei Tan was born in Hunan, China, in 1999. He received the B.S. and M.S. degrees in electrical engineering in 2021 and 2024, respectively, from Central South University, Changsha, China, where he is currently working toward the Ph.D. degree in control science and engineering.

His research interests include wireless power transfer and power electronics.

Mr. Tan was a recipient of the Top 10 First Stage Proposal Award in the Inaugural IEEE Global Student Wireless Power Competition in 2022.

Zixi Liu (Member, IEEE) received the B.S. degree in electrical engineering and automation from Sichuan University, Chengdu, China, in 2016, the M.S. degree in software engineering, and the Ph.D. degree in control science and engineering from Central South University, Changsha, China, in 2019 and 2023, respectively.

His research interests include wireless power transfer and power electronics and renewable energy.

Dr. Liu was a recipient of the Top 10 First Stage Proposal Award in the Inaugural IEEE Global Student Wireless Power Competition in 2022. Since 2023, he has been a Senior Hardware Research and Development Engineer with Xiaomi, Beijing, China.

Qi Zhu received the B.S. degree in electrical engineering and automation and the Ph.D. degree in control science and engineering from Central South University, Changsha, China, in 2014 and 2019, respectively.

He was a joint Ph.D. student from 2017 to 2019 and a Research Fellow from 2019 to 2021 both under the supervision of Prof. A. Patrick Hu with the University of Auckland, Auckland, New Zealand. Since 2022, he has been a Senior Hardware Research and Development Engineer with Xiaomi, Beijing, China. His research interests include wireless power transfer, power electronics, and renewable energy.

Yao Sun (Member, IEEE) was born in Hunan, China, in 1981. He received the B.S. degree in automation, the M.S. degree in control science and engineering, and the Ph.D. degree in control science and engineering from Central South University, Changsha, China, in 2004, 2007, and 2010, respectively.

He has been a Professor with the School of Automation, Central South University, China. His research interests include matrix converters, microgrids, and wind energy conversion systems.

Mei Su (Member, IEEE) was born in Hunan, China, in 1967. She received the B.S. and M.S. degrees in automation and the Ph.D. degree in control theory and control engineering from the School of Information Science and Engineering, Central South University, Changsha, China, in 1989, 1992, and 2005, respectively.

She was a Full Professor with the School of Automation, Central South University. Her research interests include matrix converter, adjustable speed drives, and wind energy conversion system.

Dr. Su is currently an Associate Editor for IEEE TRANSACTIONS ON POWER ELECTRONICS and IEEE TRANSACTIONS ON SUSTAINABLE ENERGY.

Bo Long received the B.Tech. degree in optoelectronics and the M.E. and Ph.D. degrees in electrical and electronics engineering from The University of Auckland, Auckland, New Zealand, in 2014, 2017, and 2024, respectively.

In 2025, he was with Xiaomi Inc., as a Senior Staff Hardware Engineer to develop innovative smartphone wireless power transfer technologies. His research interests include wireless power transfer, foreign object detection, and power electronics.